Interactive Radial Volume Histogram Stacks for Visualization of Kidneys from CT and MRI

M. Alper Selver
Dokuz Eylül University
Dept. of Electrical and Electronics Engineering, Tınaztepe Campus
35160, Buca, Izmir, TURKEY
alper.selver@deu.edu.tr

Merve Özdemir
Dokuz Eylül University
Institute of Natural and Applied Sciences, Tınaztepe Campus
35160, Buca, Izmir, TURKEY
merveozdemir89@gmail.com

Eşref Selvi
Dokuz Eylül University
Institute of Natural and Applied Sciences, Tınaztepe Campus
35160, Buca, Izmir, TURKEY
esref.selvi@hotmail.com

ABSTRACT

Optical parameter assignment via Transfer Functions (TF) is the sole interactive part in medical visualization via volume rendering. Being an interactive element of the rendering pipeline, TF specification has very important effects on the quality of volume-rendered medical images. However, TF specification should be supported by informative search spaces, interactive data exploration tools and intuitive user interfaces. Due to the trade-off between user control and TF domain complexity, integrating different features into the TF without losing user interaction is a challenging task since both are needed to fulfill the expectations of a physician. By addressing this problem, we introduce a semi-automatic method for initial generation of TFs. The proposed method extends the concept of recently introduced Volume Histogram Stack (VHS), which is a new domain constructed by aligning the histograms of the image slices of a CT and/or MR series. In this study, the VHS concept is extended by allowing the user to define an alignment axis using orthogonal multi planar reconstructions via simple, yet effective, interaction mechanisms. The construction of VHS according to the slices generated specifically for user defined search space allows the more informative integration of local intensity distribution, and better spatial positioning of the organ of interest into the TF. For testing, the proposed strategy is applied to kidney visualization from CT and MRI series. The performance of extended VHS domain is evaluated via intensity based TF design. Volumetric histogram based manual TF specifications are quantitatively compared to VHS based manual tweaking of original slices, and to extended-VHS based automatic TF design. The results show both quantitatively and qualitatively enhanced rendering quality for kidney visualization.

Keywords

Transfer Function Specification, Volume Rendering, Medical Visualization, Kidney.

INTRODUCTION

Visualization aims to produce clear and informative pictures of the important structures in a data set. Depending on the application, this requires interactive determination of visual parameters such as opacity and color. In volume rendering technique [Dre98], combinations of these visual parameters can be determined during the rendering pipeline. During the generation of volume rendered images, Transfer Function (TF) specification is the step where these adjustments can be done. Therefore, it is crucial and important to design accurate TFs to produce meaningful and intelligible 3-D images. However, TF design is a very difficult task because of the availability of various possibilities in extensive search spaces of TFs [Pfi00]. Since this flexibility of search space cannot be kept in strict bounds, specification of an appropriate TF is a challenging problem, where effective initial TF designs should be generated prior to the optimization part, which is controlled by the user. Moreover, advanced user interaction interfaces [Rez06] and data exploration tools [Sel07] should be provided for fulfilling user expectations.

To overcome the difficulty of initial TF generation generally a number of predefined TF presets are used as starting point (so called initial TF design). The main idea behind this approach is that certain types of volume data are standardized in the range of data values and special sub-ranges are assigned to the same type of structure (thus, predefined TFs are adjusted due to these ranges). However, volumetric data usually have varying characteristics even in different samples of the same application. For instance, in medical imaging, depending on different modality settings, injection of a contrast media or environmental circumstances, the sub-ranges of the tissues may vary significantly. For these reasons, a limited number of TF presets cannot be enough to cover all possible cases and to provide useful initial

 ISBN 978-80-86943-74-9

TFs. In order to create a useful initial TF that provides a good basis prior to optimization, an automatic sub-range detection method that finds the intensity range for each structure of interest is needed. Moreover, it is necessary to integrate the developed method into the TF design procedure without losing user control and interaction over the search space.

TF specification methods can roughly be divided into two groups as data-centric [Kin98] and image-centric [Shi98]. In both of them, finding the contours that are hidden behind another is an important aspect of useful TF generation [Baj97]. To achieve this goal, effective use of spatial information is necessary [Roe05]. In [Roe05], spatial TFs are introduced as 1D or multidimensional TFs, where spatial information has been used to derive the color, whereas statistical (and/or spatial information) is used to set up the opacity. Local properties are used to increase the performance of topological approaches. In [Sat00], 3D filters, based on gradient vector and Hessian matrix, are used to enhance specific 3D local intensity structures. In [Lun06a], histogram contents for local neighborhoods are used to detect and separate tissues with similar intensities. In [Lun06b], an enhancement that amplifies ranges corresponding to spatially coherent materials by using alpha-histograms, which are individually retrieved by dividing the data set into local regions, is implemented. These studies show the importance of local information in solving major problems in TF generation such as the classification of overlapping tissues. Recent studies also focus on size [Wes10], shape, appearance [Saa10] and visibility [Car11] of anatomical structures for constructing effective TFs.

By addressing this problem, we introduce a semi-automatic method for initial generation of TFs. The proposed method extends the concept of Volume Histogram Stack (VHS). VHS is recently introduced in [Sel09] as a new domain which is created by aligning the histograms of the image slices of a CT/MR series. Histograms were generated from orthogonal directions of slice planes, namely, axial, coronal and sagittal. Thus, VHS can represent the intensity values of the tissues as well as their spatial information and local distributions (via lobes in VHS) which are not available in conventional volume histograms. The tissues which are at different slices but with similar gray level distributions can clearly be distinguished by using this spatial information. Then, a tissue (a structure of interest) can effectively be visualized by determining its corresponding lobe(s) in VHS, which represents that structure of interest, and by assigning a color-opacity value to that lobe.

In this study, the VHS concept is extended by allowing user to define an alignment axis using orthogonal multi planar reconstructions via simple, yet effective, interaction mechanisms. The construction of VHS according to aligning the slices generated specifically for user defined search space allows the integration of local intensity distribution, and spatial positioning of the organ of interest into the TF. For testing, the proposed strategy is applied to kidney visualization from CT and MRI series. The performance of extended VHS domain is evaluated via intensity based TF design. Volumetric histogram based manual TF specifications are quantitatively compared to VHS based manual tweaking of original slices, and extended VHS based automatic TF design. The results show both quantitatively and qualitatively enhanced rendering quality for kidney visualization. With the help of this expansion, the VHS becomes an effective new domain as a search space for TF specification on any kind of 3D data.

DATA SETS

The first application is an abdominal CT series taken at the venous phase for the evaluation of a liver transplantation donor [Sel07] (Figure 1). Images were acquired after contrast agent injection at portal phase using a Philips Secura CT with two detectors equipped with the spiral CTA option and located in Dokuz Eylül University Radiology Department. The second data set is acquired using a 1,5T MRI system located in the same department. Both scanners produce 12 bit DICOM images with a resolution of 512 × 512 for CT and 256 x 256 for MR. The data sets were collected from the Picture Archiving and Communication System of the same department.

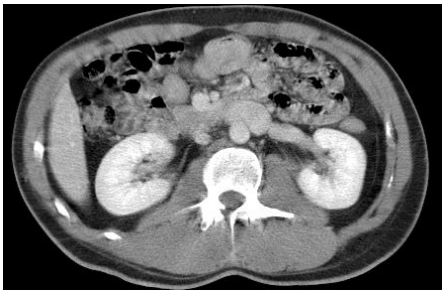

(a)

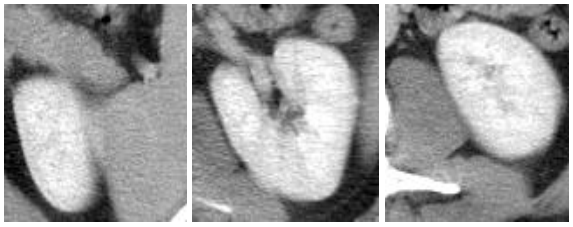

(b)

Figure 1. a) An original CT image slice (direction of acquisition), (b) Left kidneys at different slices (left to right order is from beginning to the end of the series). Note that, kidney start to occur smaller, becomes larger and gets smaller again.

 ISBN 978-80-86943-74-9

METHODOLOGY

In CT and/or MR data sets, the kidneys may have different gray value distributions according to environmental circumstances, injection of a contrast media, and certain modality parameters. Moreover, their location, orientation and size may differ due to patient anatomy (Figure 1). Although, there is a calibrated intensity scale in CT (i.e. Hounsfield Units – HU), the above mentioned diversity still exists. Moreover, volume rendering is not commonly used for MR data sets since there is no calibrated intensity scale. In conventional approach, both for CT and MR data sets, the volume histogram is the main guide to find the tissues of interest.

On the other hand, these kidneys do not always correspond to visible peaks as reported in [Lun06a]. The reason behind this is the existence of dominant peaks which occur due to unified intensity range of overlapping tissues such as liver and spleen. Especially in CT, these abdominal organs occur in a very narrow range of HU values. This overlap hardens the usage of TFs in the visualization of kidneys.

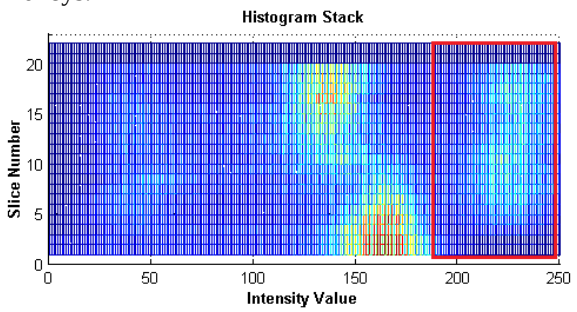

(a)

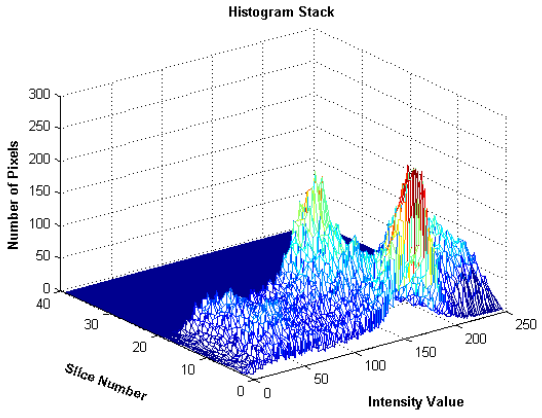

(b)

Figure 2. Left kidney analysis from CT (a) VHS for cropped axial slices (top view), red rectangle shows the intensity range of left kidney (b) VHS for axial slices (rear view).

Through a series of abdominal image slices, kidneys begin to occur as small objects at first, expand in the successive slices, and finally disappear by becoming smaller objects as slices proceed (Figure 1.b). This causes a lobe-like histogram distribution for kidneys. The peaks of the lobes are at the slices in which kidneys appear biggest in size (Figure 2). This additional information is available only if the z-dimension (orthogonal to the slices) is used as exploited in the VHS concept.

This provides the advantage of discriminating kidneys from other organs that are spatially separated in the direction of acquisition even if the intensity range of these organs/tissues completely overlap with kidneys. Traditional volume histograms cannot take this advantage as they represent cumulative gray-level distribution over all data set. On the other hand, in practice, kidneys do not get completely separate lobes. Instead, the lobes have intersecting regions if kidneys and similar intensity organs are partially spatially non-separated.

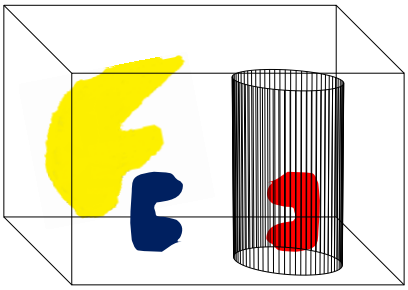

(a)

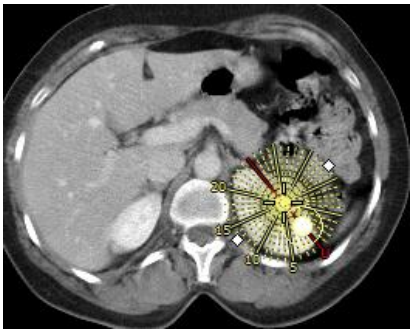

(b)

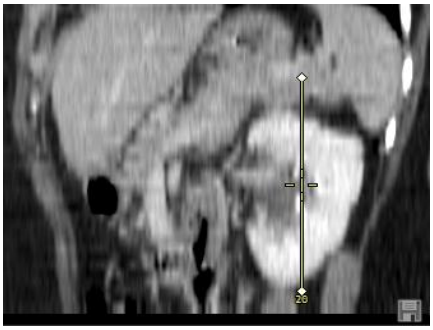

(c)

Figure 3. (a) Reconstruction strategy inside the volume, (b) circular area selection from axial, (c) vertical height selection from sagittal (left kidney)

 ISBN 978-80-86943-74-9

To take advantage of spatial knowledge more, VHS approach has been extended to produce alignments through x and y-dimensions. For instance, in the above mentioned case, if the major slicing axis is z-dimension, VHS which can be generated using the histograms calculated for axial images (x-y dimensions) and aligned through z-dimension to construct VHS. Moreover, with the help of spatial extension, VHS can also be generated by using the histograms of coronal images (y-z dimensions) and aligning them through x-dimension or the histograms of sagittal images (x-z dimensions) aligning them through y-dimension. This enables organ based selection for the VHS which can be generated based on the organ to be visualized and independent of slicing axis without an additional scanning procedure. With this opportunity, VHS can distinguish structures which are separated in any of x, y, and z-dimensions.

In this study, this approach is further extended for kidney visualization by allowing the user to select a cylindrical tube using a Multi Planar Reconstruction (MPR) interface (Figure 3.a). The interaction mechanism enables user to select a circular Region of Interest (ROI) first (Figure 3.b), in any one of three MPR reconstructions (i.e. axial, sagittal, and coronal). This step determines the center and radius of the 3-D cylinder. Then, using an MPR image, which is orthogonal to the MPR image used in the first step, the height of the cylinder is determined (Figure 3.c). Finally, based on a defined thickness, new image slices, all of which have same center position and size of (2 x radius) x height, are generated (Figure 4.a). The VHS generated using these user defined slices by aligning their histograms exploits more a priori information as providing kidney specific inter-slice spatial domain knowledge (Figure 4.b-c). Thus, the information on local histogram distributions of organ of interest is more evident (Figure 5-6). The tissues which are at different slices but with similar gray-level distributions can clearly be distinguished by using this spatial information.

The VHS data exploits more a priori information as saving inter-slice spatial domain knowledge since each slice histogram is represented separately. It demonstrates changes in the gray values through the series of slices, thus includes information on local histogram distributions of tissues. For example, when a tissue appears larger in an image, the number of pixels representing this tissue also increases and vice versa. The VHS demonstrates these changes much better than the volume histogram since the data distribution is shown in a continuous way through the series. Thus, it can represent the intensity values of the tissues as well as their spatial information and local distributions which are not available in conventional volume histograms.

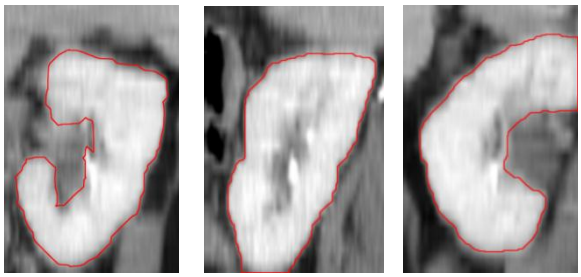

(a)

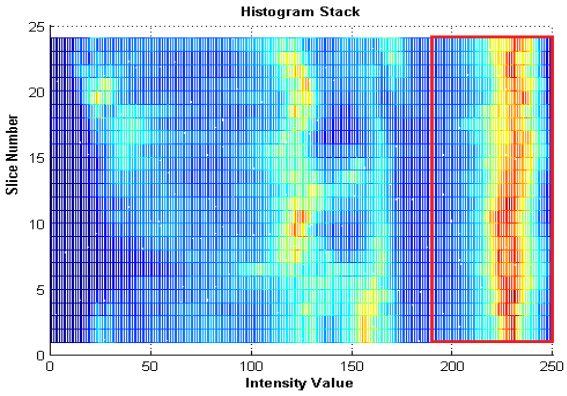

(b)

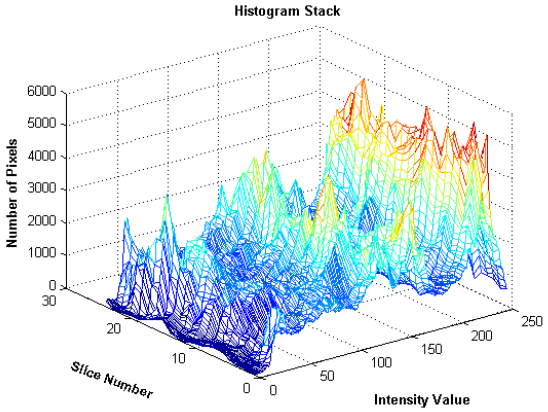

(c)

Figure 4. (a) Left kidneys at reconstructed slices (b) VHS for reconstructed slices (top view), red rectangle shows the intensity range of left kidney (c) VHS for reconstructed slices (rear view).

(a) **(b)** **(c)**

Figure 5. Axial CT Left Kidney (LK), (a) result of thresholding 185<T<250, (b) result of post-processing, (c) difference with reference.

 ISBN 978-80-86943-74-9

(a) **(b)** **(c)**

Figure 6. Reconstructed CT Left Kidney (LK), (a) result of thresholding 200<T<250, (b) result of post-processing, (c) difference with reference.

RESULTS

We have tested our algorithm on both MR and CT data sets. Four data sets (i.e. 2 MR and 2 CT) consist of axial DICOM slices from abdomen, thus include both left and right kidneys. First, we obtained the VHS of both axial and reconstructed images of left and right kidneys. Then, for both VHS, a threshold range is determined manually. According to the indicated threshold range, an intensity based TF is designed and pixels are classified. A simple post-processing part has been used which uses "connected component" analysis. With the help of post-processing, small misclassifications (Figure 10. b, f, j, n, s, w) are eliminated by selecting largest connected component (Figure 10. c, g, k, o, t, y).

Accuracy of classifications is compared with reference data sets, which were manually segmented. The same procedure is also applied to axial data sets and results are compared. Considering each pixel is either assigned to kidney (i.e. Positive - 1) or not (Negative - 0), the comparisons are made by counting True Positive (TP), True Negative (TN), False Positive (FP), and False Negative (FN) instances. The error measures calculated between classification results and reference data using above variables are:

1) False Positive Ratio (FPR =100*FP / (TN+TP)),
2) False Negative Ratio (FNR =100*FN / (TP+FN)),
3) Sensitivity, which gives the percentage of positive labeled instances that were predicted as positive, and calculated as (SE =100*TP / (TP+FN)),
4) Specificity, which gives the percentage of negative labeled instances that were predicted as negative and calculated as (SP =100*TN / (TN+FP)),
5) Positive Predictive Value (i.e. Precision), which gives the percentage of positive predictions that are correct and calculated as (PPV =100*TP / (TP+FP)),
6) Negative Predictive Value, which gives the percentage of negative predictions that are correct and calculated as (NPV =100*TN / (TN+FN)).

The values of these measures are given in Tables 1-3.

	Organ	Data Type	FPR	FNR	SE	SP	PPV	NPV
CT Data set	LK	Axial	0.17	14.65	85.35	99.72	99.58	89.82
		Reconst.	0.23	15.86	84.14	99.70	99.13	93.80
	RK	Axial	0.52	13.27	86.73	99.27	97.96	95.05
		Reconst.	0.49	12.56	87.44	99.28	98.50	93.76
MR Data set	LK	Axial	10.29	28.03	71.97	91.21	85.15	88.29
		Reconst.	2.51	18.98	81.02	96.36	93.69	89.44
	RK	Axial	0.08	20.46	79.54	99.89	99.71	91.52
		Reconst.	0.53	9.50	90.50	99.06	98.81	92.40

Table 1. Kidneys Results for Axial and Reconstructed CT and MR Data set without post-processing

	Organ	Data Type	FPR	FNR	SE	SP	PPV	NPV
CT Data set	LK	Axial	6.63	25.97	74.03	90.47	85.70	81.80
		Reconst.	1.57	15.76	84.24	97.92	91.73	93.75
	RK	Axial	4.60	13.08	86.92	94.56	85.54	94.89
		Reconst.	5.13	11.64	88.36	93.23	88.01	93.74
MR Data set	LK	Axial	13.15	27.81	72.19	87.32	79.83	87.97
		Reconst.	14.63	18.96	81.04	81.31	73.89	88.01
	RK	Axial	1.55	19.63	80.37	97.85	94.79	91.63
		Reconst.	0.74	9.38	90.62	98.71	98.32	92.46

Table 2. Kidneys Results for Axial and Reconstructed CT and MR Data set with post-processing

 ISBN 978-80-86943-74-9

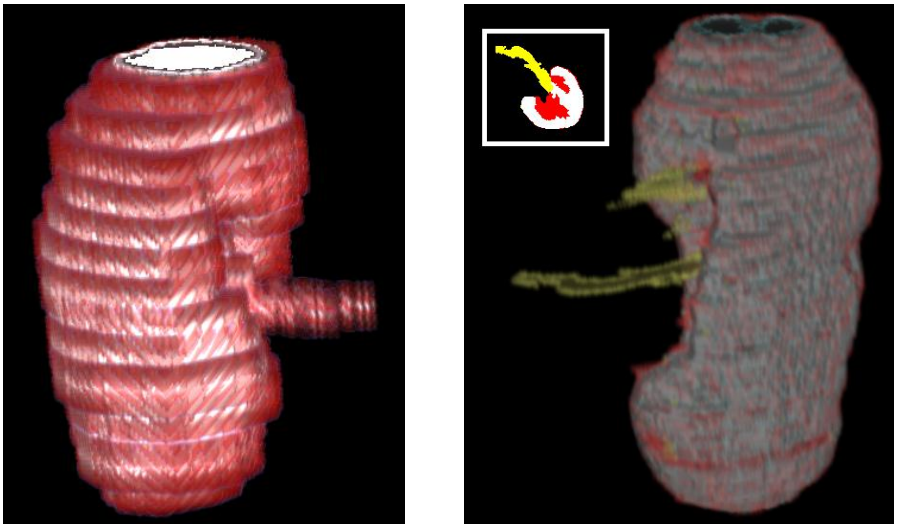

(a) **(b)**

Figure 7. 3D reconstruction of axial image of (a) MR right kidney, (b) CT left kidney.

In Table 1-2, the results of first CT - MR data set pair are given for axial and reconstructed images. These data sets differ from the second CT - MR data set pair in terms of image contrast. In other words, histogram of first CT-MR data set pair is narrower than the histogram of second CT-MR data set pair.
In Table 1, application of proposed algorithm without post-processing is given, while Table 2 covers results with post-processing.

The results show comparable performance for left kidney (LK) of axial and reconstructed VHS for CT data. On the other hand, results for MR data show improved performance especially when no post-processing is done. This is an important result since it shows better data classification on reconstructed TF domain than axial TF domain.

Considering right kidney (RK) (i.e. 3^{rd} and 4^{th} rows), the results show that FPR values are comparable but FNR measures are significantly better using reconstructed VHS for CT data. The results for MR data set (i.e. 7^{th} and 8^{th} rows) are. Similar to the results in CT, error measures show significantly improved FP and FN rates using reconstructed VHS domain.

The selection of the orientation and size of radial reconstruction for VHS is shown in Figure 8. In Figure 9, VHS for both axial and reconstructed data and manually determined threshold ranges are shown. Figure 10 shows slice-by-slice results for a set of selected images.

Table 3 shows the results of error measures for second CT - MR data set pair. For CT data, FNR rate is significantly reduced for bot LK and RK using reconstructed VHS domain. Moreover, for MR data set, both FPR and FNR are lower when reconstructed VHS is used. Other measures also reflect the superior performance of proposed domain compared to the original domain. Figure 11 shows slice-by-slice results for a set of selected images for these data sets. Two exemplary 3D reconstructions are given in Figure 7 (note that no-post processing filters are used to increase rendering quality to sow FP and FN voxels clearly).

CONCLUSIONS

This study presents a new domain for TF specification by extending volume histogram stacks, which are constructed by aligning histogram of each slice in a medical image series. The extension is done by using multi planar reconstructions and a user-friendly interface to determine a radial reconstruction of the original data. Although four data sets are used, the intensity TF based classification using reconstructed VHS is shown to have higher performance than using VHS for axial images. Although, these results should be confirmed by increasing number of applications, some early conclusions can be made. First, the shape of kidneys show less variability in size at reconstructed images compared to axial slices, which is an important advantage for shape based approaches. Second, in this study, reconstructed VHS are created using interpolated images (i.e. Figure 4.a, 10.e, m, v, 11.f, p, aa). However, using data without interpolation might increase the performance.

An automatic method finding appropriate intensity range of an organ of interest especially using local VHS information is a challenging future study. Also, a user interface, which can use different geometries for VHS generation, will be developed for allowing the use of VHS for other organs.

 ISBN 978-80-86943-74-9

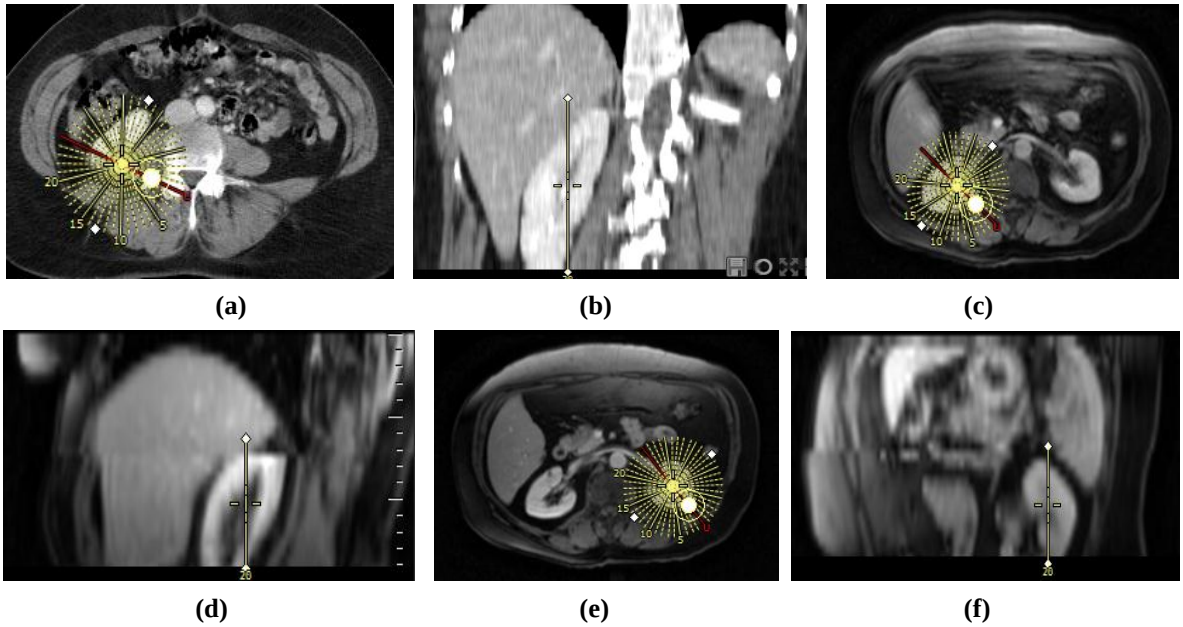

(a) (b) (c)

(d) (e) (f)

Figure 8. Circular area and vertical height selections (a, b) CT RK, (c, d) MR RK, (e, f) MR LK

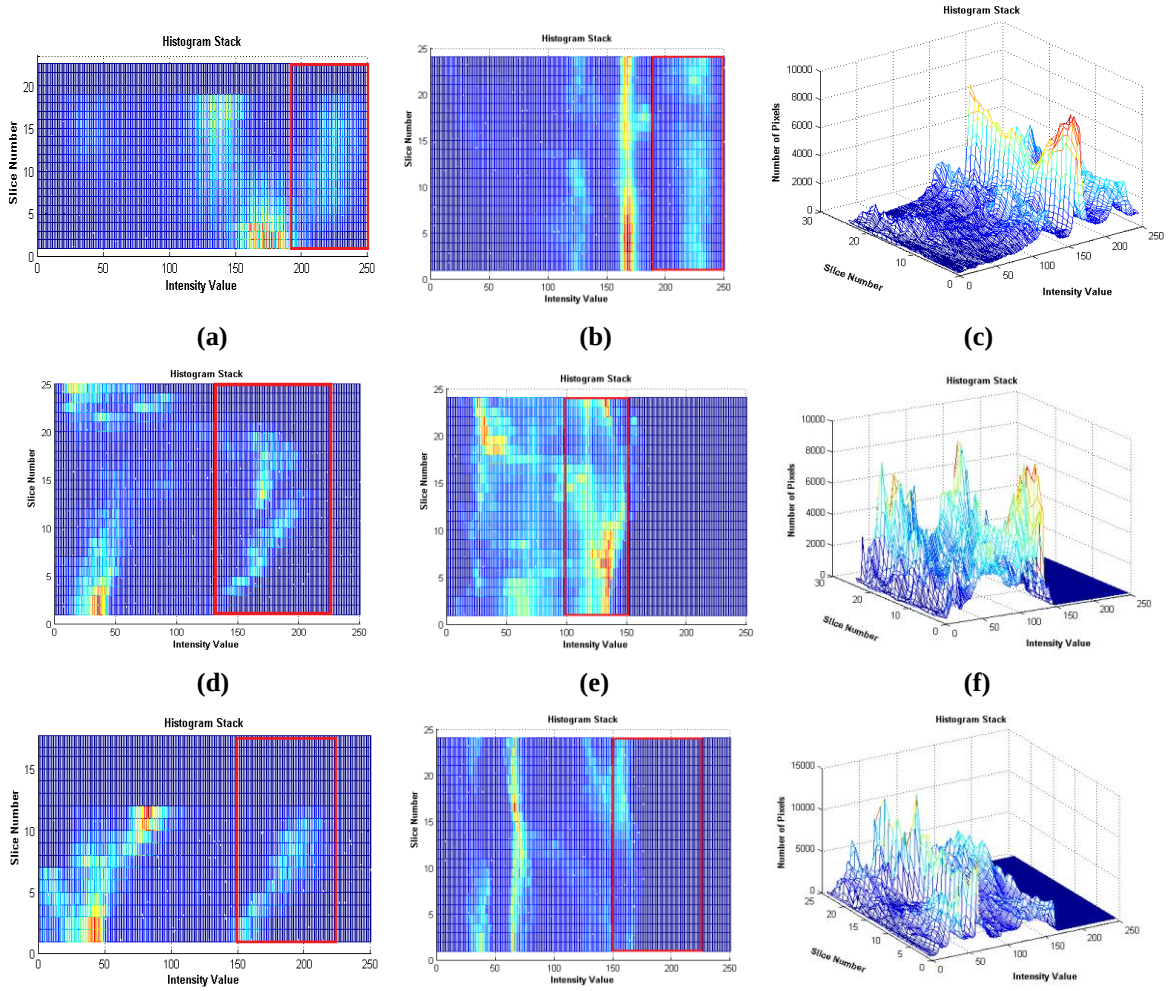

(a) (b) (c)

(d) (e) (f)

(g) (h) (i)

Figure 9. Right kidney analysis from CT (a) VHS for axial slices (top view), VHS for reconstructed slices, (b) top view, (c) side view. Left kidney analysis from MR (d) VHS for axial slices (top view), VHS for reconstructed slices, (e) top view, (f) side view. Right kidney analysis from MR (g) VHS for axial slices (top view), VHS for reconstructed slices, (h) top view, (i) side view. (*PS: red rectangles show the intensity ranges of kidneys)*.

 ISBN 978-80-86943-74-9

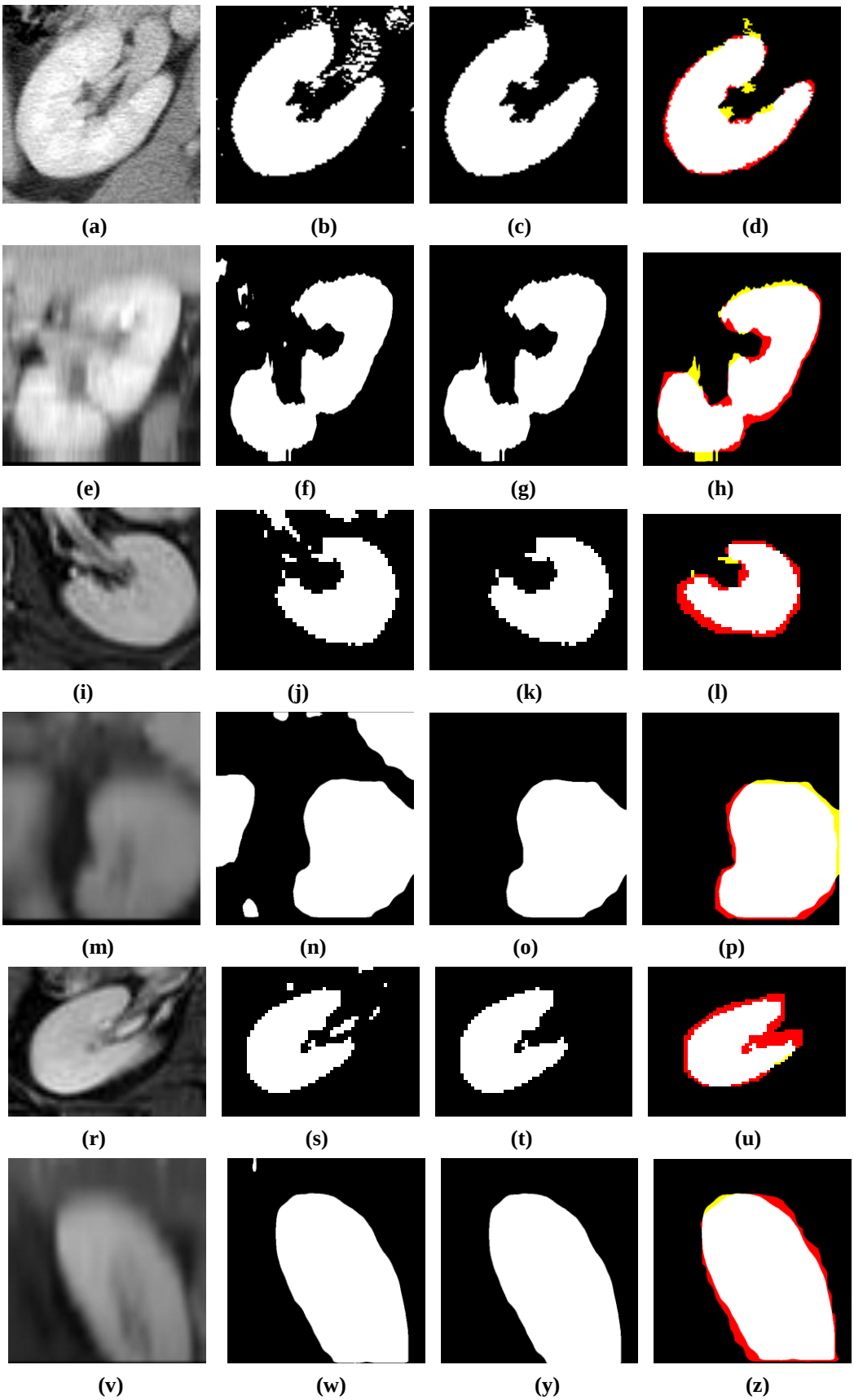

Figure 10. CT Right Kidney (RK) (a) cropped axial image, (b) result of thresholding 185<T<250, (c) result of post-processing, (d) difference with reference, (e) reconstructed image, (f) result of thresholding 185<T<250, (g) result of post-processing, (h) difference with reference. MR Left Kidney (LK) (i) cropped axial image, (j) result of thresholding 140<T<230, (k) result of post-processing, (l) difference with reference, (m) reconstructed image, (n) result of thresholding 100<T<150, (o) result of post-processing, (p) difference with reference, MR Right Kidney (RK) (r) cropped axial image, (s) result of thresholding 150<T<230, (t) result of post-processing, (u) difference with reference, (v) reconstructed image, (w) result of thresholding 100<T<180, (y) result of post-processing, (z) difference with reference.

 ISBN 978-80-86943-74-9

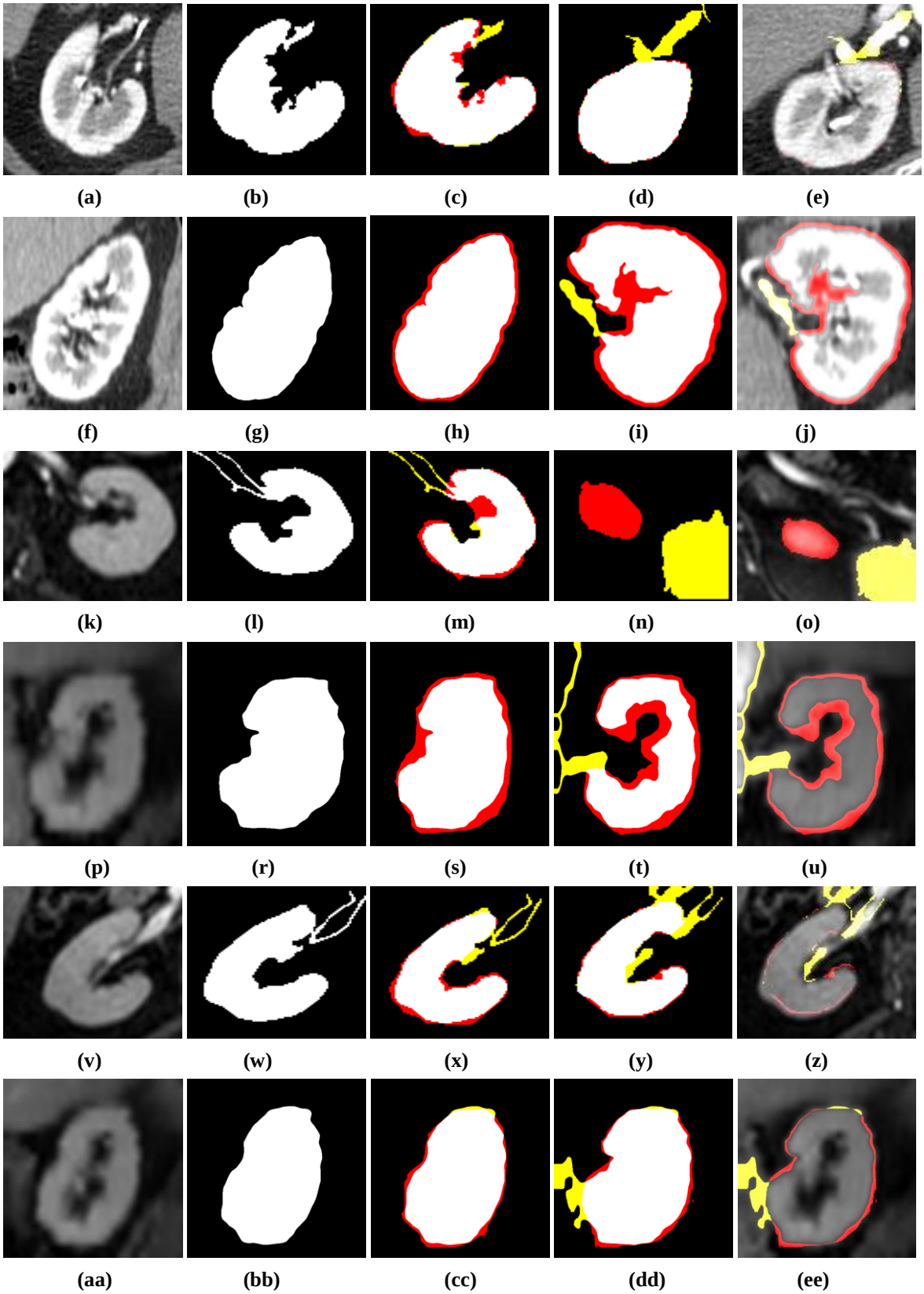

Figure 11. For all rows of the figure, from left to right, the images show: cropped axial or reconstructed image, result of post-processing, difference of result with reference, another example of difference image from the same data set, transparent illustration of FP and FN pixels on the image. The rows of the figure correspond to (a)-(e) axial CT Right Kidney, (f)-(j) reconstructed CT Right Kidney, (k)-(0) axial MR Left Kidney, (p)-(u) reconstructed MR Left Kidney, (v)-(z) axial MR Right Kidney,(aa)-(ee) reconstructed MR Right Kidney (*FP pixels are shown in yellow while FN pixels are shown in red*).

 ISBN 978-80-86943-74-9

	Organ	Data Type	FPR	FNR	SE	SP	PPV	NPV
CT Data set	LK	Axial	0.39	22.43	77.57	99.55	98.17	94.47
		Reconst.	0.75	4.4	95.6	99.1	96.72	98.73
	RK	Axial	0.86	8.13	91.87	98.9	96.7	97.83
		Reconst.	2.89	5.62	94.38	97.06	88.54	97.31
MR Data set	LK	Axial	1.05	22.32	77.68	98.99	93.06	96.31
		Reconst.	0.18	22.69	77.31	99.77	99.43	89.77
	RK	Axial	0.78	10.78	89.22	99.02	96.83	97.51
		Reconst.	0.58	10.48	89.52	99.17	98.38	94.81

Table 3. Kidneys Results for Axial and Reconstructed CT and MR Data set with post-processing

ACKNOWLEDGMENTS

This study is supported by TUBITAK EEEAG under grant number 112E032.

REFERENCES

[Baj97] Bajaj, C.L., Pascucci, V., Schikore, D.R., "The Contour Spectrum," Proc. Eighth IEEE Visualization Conf. (VIS '97), pp. 167-173, 1997.

[Car11] Carlos D. C., Kwan-L. M., "Visibility Histograms and Visibility-Driven Transfer Functions," IEEE Transactions on Visulization and Computer Graphics, 17(2), 192-204, 2011.

[Dre98] Drebin RA, Carpenter L, Hanrahan P, "Volume Rendering," Proc. ACM SIGGRAPH '88, pp. 65-74, 1988.

[Kin98] Kindlmann, G., Durkin, J.W., "Semi-Automatic Generation of Transfer Functions for Direct Volume Rendering," Proc. Ninth IEEE Visualization Conf. (VIS '98), pp. 79-86, 1998.

[Lun06a] Lundström, C., Ljung. P., Ynnerman, A., "Local Histograms for Design of Transfer Functions in Direct Volume Rendering," IEEE Transaction on Visualization and Computer Graphics, vol. 12(6), 1570-1579, Nov./Dec. 2006.

[Lun06b] Lundström, C., Ynnerman, A., Ljung, P., Persson, A., Knutsson, H., "The Alpha-Histogram: Using Spatial Coherence to Enhance Histograms and Transfer Function Design," Proc. Eurographics/IEEE-VGTC Symp. 2006.

[Pfi00] Pfister, H., Lorensen, B., Bajaj, C., Kindlmann, G., Schroeder, W., Machiraju, R., "The Transfer Function Bake-Off," Proc. 11th IEEE Visualization Conf. (VIS), 523-526, 2000.

[Rez06] Rezk Salama C., Keller M., Kohlmann P., "High-Level User Interfaces for Transfer Function Design with Semantics," IEEE Trans. Visualization and Computer Graphics, vol. 12, Issue: 5, Page(s):1021-1028, Sept./Oct. 2006.

[Roe05] Roettger, S., Bauer, M., Stamminger, M., "Spatialized Transfer Functions," Proc. Eurographics/IEEE-VGTC Symp. Visualization (EuroVis '05), pp. 271-278, 2005.

[Saa10] Saad A., Hamarneh G., Moller T., "Exploration and Visualization of Segmentation Uncertainty Using Shape and Appearance Prior Information," IEEE Transactions on Visulization and Computer Graphics, vol. 16, Issue:6, Page(s):1366-1375, November-December 2010.

[Sat00] Sato Y, Westin CF, Bhalerao A, Nakajima S, Shiraga N, Tamura S, Kikinis R, "Tissue Classification Based on 3D Local Intensity Structures for Volume Rendering," IEEE Transaction Visualization and Computer Graphics, 6(2), 160-180, Apr.-June 2000.

[Sel07] Selver M.A., Fischer F., Kuntalp M., Hillen W., "A Software Tool for Interactive Generation, Representation, and Systematical to range of Transfer Functions for 3D Medical Images," Comp. Meth. Prog. Biomed., 86, 270-280, 2007.

[Sel08] Selver M.A., Kocaoglu A., Demir G., Dogan H., Dicle O., Guzelis C., "Patient Oriented and Robust Automatic Liver Segmentation for Pre-Evaluation of Liver Transplantation," Computers in Biology and Medicine, 38(7),:765-784, 2008.

[Sel09] Selver M.A., Guzelis C., "Semiautomatic Transfer Function Initialization for Abdominal Visualization Using Self-Generating Hierarchical Radial Basis Function Networks" IEEE Transaction on Visualization and Computer Graphics, 15(3), 395-409, May/June 2009.

[Shi98] Shiaofen, F., Tom, B., Mihran, T., "Image-Based Transfer Function Design for Data Exploration in Volume Visualization," Proc. Ninth IEEE Visualization Conf.. 319-326, 1998.

[Wes10] Wesarg S., Kirschner M., Khan M. F., "2D Histogram based volume visualization: combining intensity and size of anatomical structures," International Journal of Computer Assisted Radiology and Surgery, vol. 5, Page(s): 655–666, May 2010.